Engineering Structures 272 (2022) 114965

Contents lists available at ScienceDirect

Engineering Structures

journal homepage: www.elsevier.com/locate/engstruct

Artificial Neural Network-based Finite Element method for assessing fatigue and stability of an origami-inspired structure

Mojtaba Moshtaghzadeh [a,1], Ali Bakhtiari [b,2], Pezhman Mardanpour [a,*,3]

[a] Department of Mechanical and Material Engineering, Florida International University, Miami, FL, 33174, USA
[b] Department of Civil and Environmental Engineering, Florida International University, Miami, FL, 33174, USA

ARTICLE INFO

Keywords:
Stability
Fatigue
Origami
Reconfigurable structure
Kresling pattern
FEM
ANN

ABSTRACT

In this paper, we present a comprehensive study of mechanical characteristics of a reconfigurable origami-inspired structure using Finite Element and Artificial Neural Network (ANN) approaches. We introduce a design of crease section in the proposed reconfigurable structure, which undergoes enormous and complicated deformation in the folding and unfolding process. Although this crease design can make the deploying process more straightforward, it can jeopardize the stability and life cycle of the structure. We explore how the geometric parameters of the design affect the stability and fatigue failure, including length ratio, total height, story's height, thickness, crease indexes, and circumscribed circle's radius. In order to reduce the computational time, we develop an ANN employing the obtained Finite Element method (FEM) results. The ANN results demonstrate that decreasing the circumscribed circle's radius, the length ratio, and the total height enhance the stability of the origami-inspired structure. It is found that crease indexes affect stability based on the radius of the circumscribed circle. In addition, we investigate how these parameters simultaneously contribute to this design's buckling load and life cycle. The results provide a detailed design parameter characteristic map that can be used to optimize origami structure performance.

1. Introduction

Origami techniques can be used to fabricate a three-dimensional model from a plane design by employing certain folding lines (creases). Minimum assembling procedure, predictable motion, and simple fabrication process are some of the advantages of origami patterns. The kinematics of origami patterns influences the origami-inspired mechanisms. The configuration of creases defines the origami-inspired structure patterns, which serve as hinges to accomplish motion from a flat sheet.

In recent decades, the origami-inspired structures have been employed in design of various engineering systems including aerospace mechanism [1], robotic [2], biomedical [3], material [4], antenna [5], architecture [6], etc. [7,8]. Bobbert et al. [3] proposed a new design of foldable orthopedic implants using origami techniques. Pesenti et al. [9] used origami shapes to design adaptive shadings in terms of the thermal and visual comfort of a building. Lee et al. [10] designed a soft robot with transformable origami wheels that can adapt to various difficult circumstances and environments as well as provide enough stiffness to keep performance at a high level. Zirbel et al. [11] studied a new approach for deploying a large solar array from a compact folded form in space application inspired by an origami pattern. By using the Kresling origami pattern, Zekios et al. [5] developed a deployable helical antenna that meets the requirements of both mechanical and electromagnetic performance. Recent years have seen an increase in origami applications, which suggests that this field requires special attention.

Cylindrical structures (thin-walled) are often employed in engineering designs which have a significant role in the design's performance [12,13]. Some cylindrical origami patterns can be able to support uniaxial expansion or compression loads along with providing tunable mechanical behavior [14]. It is shown that origami structures can be more stable in comparison with regular tubes [15]. The arrangement of faces and creases describes the cylindrical origami pattern. The Yoshimura pattern is an example of a cylindrical origami structure that can be folded axially [16,17]. Although it can be folded by twisting the structure, it is not practical for foldable designs due to the large in-plane deformations [18,19].

* Corresponding author.
E-mail addresses: mmosh009@fiu.edu (M. Moshtaghzadeh), abakh003@fiu.edu (A. Bakhtiari), Pezhman.Mardanpour@fiu.edu (P. Mardanpour).
[1] Graduate Research Assistant.
[2] Graduate Research Assistant.
[3] Associate Professor.

https://doi.org/10.1016/j.engstruct.2022.114965
Received 7 April 2022; Received in revised form 29 August 2022; Accepted 11 September 2022
Available online 23 September 2022

Nomenclature

H	Total height of structure
n	Polygon sides
R	Circumscribed circle's radius
b/a	Length ratio
h	Story's height
a, b, c	Triangle's sides
t	Thickness
δ	Angle by the horizontal surface and b
θ	Rotational angle between the bottom and topplanes
σ_a	Alternating stress
σ_m	Mean stress
α	Crease index (aspect ratio)
β	Crease index (thickness ratio)
N	Safety factor
S_e	Endurance limit
S_u	Ultimate tensile strength
E	Young's modulus
ρ	Density
ϵ	Poisson's ratio
μ_1	1st order Ogden model-material constant
α_1	1st order Ogden model-material constant
K	Stiffness matrix
§	Stress stiffness matrix
λ_i	ith eigenvalue of displacement
ψ_i	ith eigenvector of displacement
y_j	Produced output in jth layer
x_i	Input from previous layer in ith layer
σ	Activation function
w_{ij}	Interconnected weight in j and i layers
b_j	Bias
n	Quantity of samples
e_k	Output error

The Kresling is another type of cylindrical origami pattern, which includes a thin tube configuration. Due to its unique twisted configuration, this pattern is capable of folding under axial loads [20,21]. Jianguo et al. [19,22] studied a cylindrical structure inspired by the Kresling origami pattern. They discovered that changing geometric parameters influences the stability of a Kresling origami-inspired structure. Li et al. [23] utilized the Kresling origami pattern to significantly reduce the critical force of a thin-walled structure. Masana and Daqaq [24] found that geometric parameters affect the mechanical characteristics of foldable Kresling origami springs.

It is required to examine the mechanical characteristics of a reconfigurable origami-inspired structure to assess the design's performance. In addition, several important aspects should be considered in the design stage. The origami-inspired structure should be adjustable, reconfigurable, foldable, self-actuation, and easy to manufacture. The analysis of origami structure can be challenging due to the significant strain changes that occur along folding lines. Consequently, mathematics has been extensively used to design and optimize reconfigurable structures [8,25–27].

Prior studies provided several approaches, such as integrated geometric-graph-theoretic, hing and bar, and rigid folding [28–31]. It is shown that a combination of hing and bar in crease sections and springs in the panels can determine the bending deformation [32]. Chen and Feng [33] developed a nonlinear iterative strategy to predict the rigid folding characteristics of deployable origami structures based on a pin-jointed model. Hernandez et al. [34] used the smooth fold methodology to study the structure's folding behavior. A geometric-graph-theoric approach and a graph-theoretic cycle detection algorithm are employed to automatically find the crease sections in an origami structure [35].

External loads are usually applied to reconfigurable cylindrical origami structures in order to change their state, which can jeopardize the stability and endurance of the structure. The origami structures have mostly been studied from a kinematic and quasi-static perspective, and no consideration has been given to the full range of degrees of freedom. As a result, a comprehensive study should provide a description of the mechanical properties of origami-inspired structures. Qui et al. [36] presented a technique to capture a deformed origami structure's reaction force, which was considered a redundantly actuated parallel model.

Moshtaghzadeh et al. [37] developed a numerical platform using the geometrically exact, fully intrinsic nonlinear composite beam theory of Hodges [38] to investigate the stability of a Kresling origami-inspired antenna. Compared to commercial Finite Element Analysis (FEA) software, this numerical platform is proven to be much more computationally efficient for simulating complicated geometries. They showed that the structure's stability is enhanced with the increase of polygon sides. Although it is demonstrated that the obtained results are in agreement with ANSYS software results, the results are valid when the structure is beam-like. Therefore, a suitable and computationally efficient approach should be considered to present a thorough stability analysis of origami structures for a broader range of independent parameters.

There has been an enhancement in the productivity of origami designs in recent years resulting from innovations in crease designs [4]. Moshtaghzadeh et al. [39–41] presented a comprehensive fatigue study of a Kresling origami-inspired structure. They showed that utilizing flexible materials in creases can substantially postpone fatigue failure. In addition, they discussed the influence of different design parameters of a Kresling origami structure on fatigue life. The results indicate that the length ratio affects the number of stories' influence on the proposed design's fatigue life. The design's life cycles can be extended by increasing the circumscribed circle's radius. In addition, it is explored that the crease thickness considerably impacts the fatigue failure of the origami structure [40].

Although FEA and experimental studies can conduct a comprehensive mechanical analysis of a system, it can be computationally expensive due to the model's degrees of freedom. The computational time can be reduced substantially using machine learning and optimization approaches [26,42]. Upon proper training, a machine learning model is capable of predicting the output of the problem. The use of this approach has numerous applications across a wide spectrum of engineering fields, including construction [42], health care [43], energy [44], etc. [45–47]. Fan et al. [42] provided a comprehensive study of used machine learning techniques in reinforced concrete bridges. Zhang et al. [48] employed two Convolutional Neural Networks (deep learning approach) to determine the plane engineering structure's symmetry group and order.

Only a few research used the Artificial Intelligence (AI) approaches to investigate the mechanical behavior of origami structures. By comparing the input and output data, Liu et al. [49] developed an efficient strategy based on a neural-fuzzy network to identify the dynamic behavior of a multi-cell self-locking origami structure. Yasuda et al. [50] demonstrated a data-driven approach to predicting the behavior of origami unit cells using quasi-recurrent neural networks. To present an origami physical reservoir's computing capabilities, Bhovad and Li [51] used comprehensive benchmark simulations and parametric studies. They utilized artificial recurrent neural networks to investigate nonlinear origami kinematics and reservoir design.

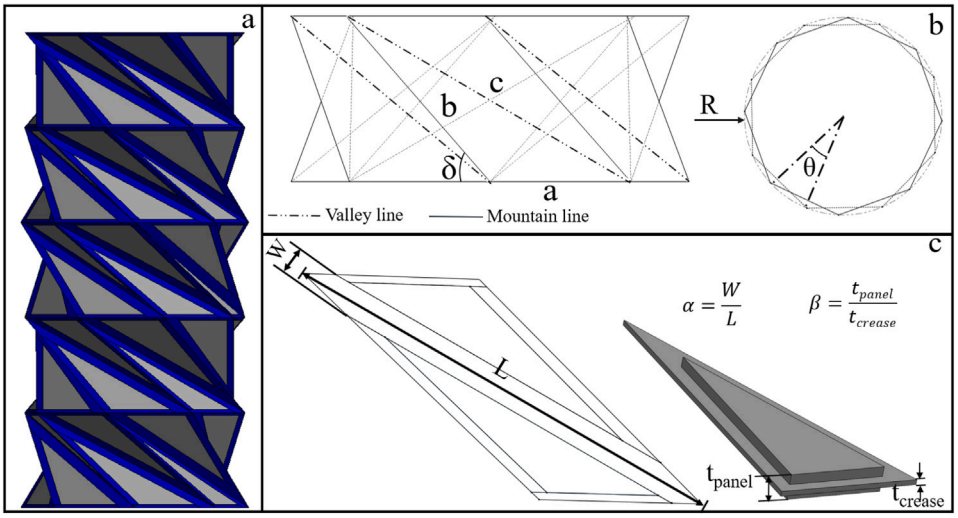

Fig. 1. (a) A five-story origami-inspired structure using Kresling pattern, (b) Kresling origami pattern geometry, (c) Crease design [40].

This paper focuses on the mechanical characteristics of an origami-inspired structure by considering the effects of various geometric parameters. Important geometric parameters which are taken into account in this study are the circumscribed circle's radius, total height, thickness, crease parameters (aspect and thickness ratios), length ratio, and story's height. We conduct this research by coupling the FEM and ANN using MATLAB and ANSYS. We develop an ANN algorithm and train it using the obtained FEM results from ANSYS software. First, the stability analysis of the structure is presented based on the predicted ANN results. Then, we find out the optimized structures by simultaneously considering the stability and fatigue failure criteria.

2. Methodology

This section provides an overview of the methods employed in this investigation. The details of the origami-inspired structure and the FEM and ANN approaches are presented.

2.1. Origami-inspired structure

This study employs the Kresling pattern to design a reconfigurable cylindrical structure. Fig. 1a presents a five-story Kresling origami-inspired structure. The geometry of the Kresling origami pattern in this research is depicted in Fig. 1b. The geometric parameters are determined as total height (H), polygon sides (n), circumscribed circle ' radius (R), thickness (t), and story's height (h). Each story includes similar triangles (valley and mountain), and their sides are defined as a, b, and c. In Fig. 1b, the valley and mountain lines are shown with dashed and solid lines, respectively. θ is the rotation of each story about the axial axis. The angle between the triangle's side (b) and the base plane is denoted by δ. Eqs. (1)–(6) represent how these parameters form the Kresling origami pattern [19,40].

$$R = \frac{\frac{a}{2}}{sin\,(\frac{\pi}{n})} \tag{1}$$

$$h = b\ sin\ \delta \tag{2}$$

$$b = \sqrt{\left[2R\ sin\ \left(\frac{2\pi/n - \theta}{2}\right)\right]^2 + (b\ sin\ \delta)^2} \tag{3}$$

$$\theta = \frac{2\pi}{n} - 2\ arcsin\ \frac{b\ cos\ \delta}{2R} \tag{4}$$

$$\frac{b}{a} \leq \frac{1}{cos\ \delta\ sin\,(\frac{\pi}{n})} \tag{5}$$

$$c = \sqrt{\left[2R\ sin\ \left(\frac{\pi}{n} + arcsin\frac{b\ cos\ \delta}{2R}\right)\right]^2 + (b\ sin\ \delta)^2} \tag{6}$$

2.2. Finite element modeling

We simulate the quasi-static folding of the origami structure using the FEA available in ANSYS software. There are two stiff planes on either side of the structure. All DOFs of the bottom plate are fixed, and the upper plate has a bonded contact with the structure. The top plate has a uniform downward linear displacement along the axial direction to predict the structure's failure under cyclic load. In order to perform stability analysis, an external axial force is applied to the upper plate of the structure.

The TARGE170 and CONTA174 elements are employed to consider the contact between the triangles' faces when the structure folds. The upper and lower triangle surfaces are considered contact (CONTA174) and target (TARFE170). The Gauss integration points method is utilized to determine the surface-to-surface contact (CONTA174) [40,52].

When the ratio of thickness to length (t/L) of a structure is much smaller than 1, the shell option is a feasible element selection in FEA. Moreover, negative Jacobian errors are less probable with this element type [53]. We discretize the model using SHELL181 available in ANSYS (four nodes structural shell element). It consists of six DOFs; transnational in x, y, and z axes and rotational about x, y, and z axes. This type of element is suitable for applications involving linear, layered, significant strain nonlinear and/or large rotation, and moderately-thick shell structures [52]. The Newton–Raphson method is used to perform this simulation, using a force convergence of 0.5% [40,52]. Ref. [40] explains in detail how this simulation does not depend on the discretization method that has been used.

The tension and compression stresses change sinusoidally through the components of the structure as it folds and unfolds. Fatigue loading is determined by the ratio between compressive and tensile stresses. A fully reserved loading condition is commonly used to assess fatigue properties, in which the ratio is −1. It means that these maximum stresses are equal, and the mean stress is zero. Afterward, a cycle of stress versus time is repeated periodically. There are two steps in a cycle, which correspond to two reversals when the loading is constant amplitude.

For fully reversed loading, determining S–N curves (alternating stress versus cycle number) requires considerable testing, and plotting curves for each combination of mean and alternating stress should be impossible. However, the Goodman diagram is an effective tool for fine-tuning this problem and predicting the fatigue failure of a structure. This study applies a fully reversed load to the origami-inspired structure to evaluate fatigue failure. When any combination of σ_a and σ_m are below or on the Goodman curve, the structure is in the safe zone (see

Eq. (9)) [52]. The details of the fatigue simulation are discussed in Refs. [39,40].

$$\sigma_a = \frac{(\sigma_{max} - \sigma_{min})}{2} \tag{7}$$

$$\sigma_m = \frac{(\sigma_{max} + \sigma_{min})}{2} \tag{8}$$

$$\frac{\sigma_a}{S_e} + \frac{\sigma_m}{S_u} = \frac{1}{N} \tag{9}$$

The instabilities of a structure can be predicted using the nonlinear-based eigenvalue buckling analysis. This approach uses the Linear Perturbation Analysis technique to predict the buckling load (bifurcation). It necessitates a pre-loaded environment that can extract solution data for the eigenvalue buckling analysis. Therefore, considering nonlinearities in the pre-loaded section can provide more accurate results than a standard linear analysis. This bifurcation buckling analysis is formulated as an eigenvalue problem using a linearized model [52].

$$\left([K] + \lambda_i[S]\right)\{\psi_i\} = \{0\} \tag{10}$$

K, S, λ_i and ψ_i represent stiffness matrix, stress stiffness matrix, ith eigenvalue, and ith eigenvector of displacements, respectively. The Block Lanczos and subspace iteration approaches determine the buckling modes in the range of negative infinity to positive infinity [52].

2.3. Crease sections

Active origami structures consist of crease and panel sections. Selecting a flexible material for crease sections can increase the DOFs, acting as an actuator in deploying or undeploying process of an origami structure. Although this process can be performed smoothly by using flexible creases, the structure encounters more complicated deformations [32]. Refs. [40,41] illustrated how the life cycle could be increased when the structure is composed of stiff panels and flexible creases.

Fig. 1a presents crease sections in blue color, and the detail of this design are shown in Fig. 1c. We define these sections with two parameters: Thickness Ratio ($\beta = t_{panel}/t_{crease}$) and Crease Aspect Ratio ($\alpha = W/L$); see Fig. 1c. The panels' material is an isotropic elastic material with the following properties: E = 1.1 × 10^3 MPa, and ϵ = 0.42, ρ = 950 kg/m^3. The 1st order Ogden model with μ_1 = 2.62 MPa and α_1 = 2.7 is used for the crease sections [54]. S–N curves of these hyperelastic and isotropic elastic materials are found using Refs. [54,55]. The detail of this design is illustrated in Refs. [39,40].

2.4. The developed artificial neural network

Data-driven methods such as ANNs can model complicated nonlinear problems with accelerated data processing. These approaches can be performed by utilizing parallel programming due to their flexible architecture (hidden layers and neurons). The ANN is extensively used as a powerful tool for system modeling in various applications such as regression, classification, time series, and anomaly detection problems [56].

The ANN's central concept is inspired by the human brain, in which the training dataset (input) is analyzed by a network of connected layers of neurons. This network is trained to perform a given assigned purpose. The trained network could then be used to perform the acquired task on any new data with adequate precision [57].

Conducting parametric studies via FEA to examine the effects of various parameters on the origami structure's stability and life cycle are not computationally efficient. Instead, the ANN approach can be a powerful predictive tool for conducting such studies. In this study, we develop an ANN to predict the origami-inspired structure's stability and life cycle based on the obtained FEM results. Arbitrarily, 70% of the dataset is considered as a training dataset, and the other 30% is used as a testing dataset. As indicated in Table 1, the network is trained by taking into account seven different parameters, including number of stories, circumscribed circle's radius, total height, panel thickness, crease thickness, crease aspect ratio, and length ratio. The life cycle and buckling load are considered to be the outputs.

Table 1
Independent parameters of the trained ANN.

Item	Feature
Feature 1	Number of stories
Feature 2	Circumscribed circle's radius
Feature 3	Total height
Feature 4	Thickness of panel
Feature 5	Thickness of crease
Feature 6	Crease aspect ratio (α)
Feature 7	Length ratio

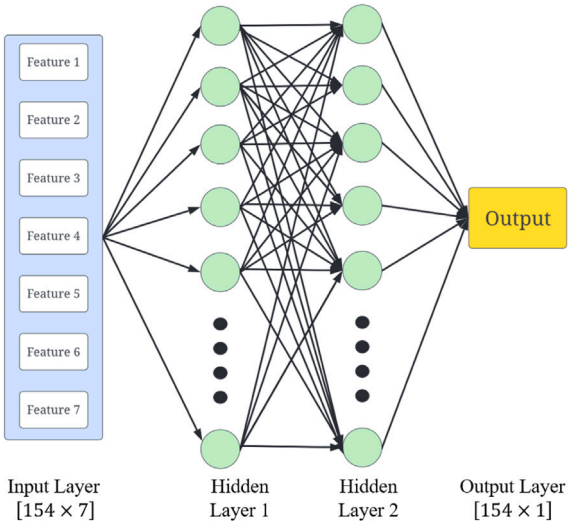

Fig. 2. The structure of the developed ANN.

Two different ANNs are trained to evaluate the stability and fatigue of this design separately. The details of the developed ANN for fatigue prediction are explained in detail in Ref. [39]. In this section, we focus on presenting the developed ANN for predicting the stability behavior of the structure. The input dataset includes 154 samples of the obtained FEM results. These geometric parameters are normalized to improve the computational efficiency and robustness of the network [39].

The developed network is shown in Fig. 2, which is comprised of three layers. Input and output layers consist of 154 × 7 and 154 × 1 matrices. In order to assess the level of accuracy of the hidden layers, we assess two to five of them. As a result, the architecture with two hidden layers delivers the lowest Root Mean Squared (RMS) errors compared with the other architectures. These hidden layers can effectively take account of the problem's nonlinearity without any potential overfitting issues [56].

The hidden layers are comprised of 20 neurons each. This number of neurons for each hidden layer is obtained by training the network 500 times. In each iteration, we find the RMS error for both datasets. The optimum case ensures a well-fitted result on the training dataset and provides generalization for the trained network. In order to achieve the target level of accuracy, hyper-parameters, including learning rate, activation function, and training algorithm are tuned through trial and error. In this way, the training ANN is guaranteed to achieve maximum accuracy while avoiding overfitting, which is crucial for proving the generalization of the ANN. Fig. 3 represents the procedure of the developed ANN and how it is trained in this study.

The training algorithm used is Levenberg–Marquardt (LM), which is an interpolation of the gradient descent and Gauss–Newton algorithms.

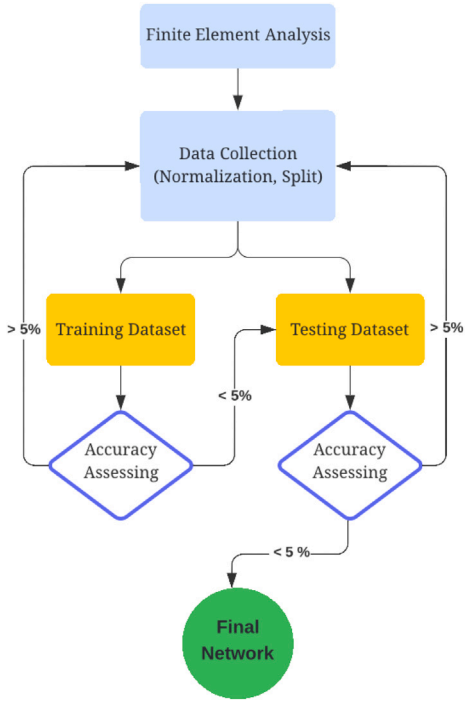

Fig. 3. The research procedure flowchart.

The learning rate applied is 0.001. In addition, 30% of the dataset is used for testing to evaluate the trained network's generalization.

According to Fig. 2, the first layer transfers the input values to the first hidden layer with corresponding weights. Neuron in each hidden layer creates and transfers an output to the next layer as the weighted sum of their inputs using Eq. (11) (hyperbolic tangent sigmoid function). This process is called feedforward. The output is computed with Eq. (11) [39,56,57].

$$\sigma_{\text{tansig}}(u) = \frac{2}{1+e^{-2u}} - 1 \tag{11}$$

$$y_j = \sigma(u_j) = \sigma\left(\sum_i w_{ij}x_i + b_j\right) \tag{12}$$

The backpropagation algorithm is utilized to calculate the optimum values of w_{ij} and b_j within the network. We calculate each iteration's RMS error with the following equation [39,56]. The gradient descent method is employed to find the minimum output error in the backpropagation algorithm. The detail of this procedure is explained in Ref. [39].

$$\text{RMS error} = \sqrt{\frac{1}{n}\sum_{k=1}^{n}(e_k)^2} \tag{13}$$

$$e_k = |\ \text{Estimated Life Cycle}_k - \text{Actual Life Cycle}_k\ | \tag{14}$$

The developed ANN is computationally intensive, as it can be learned in less than 10 s for a trial employing 10 Intel Xeon W-2155 CPU cores @ 3.30 GHz. The predicted buckling loads and life cycles compared to their actual values are shown in Figs. 4–5 for training and testing datasets. It is indicated that the predicted values are in agreement with the actual values. The predicted stability results show an average accuracy of 97.18% for the trained network. In addition, the test assessment indicates an average accuracy of 96.80%. According to Ref. [39], the trained fatigue network has accuracy with less than 1% and 2% errors for training and test sets [39]. Based on the training and testing results assessments, the developed ANNs can be utilized as an evaluation tool to conduct mechanical analysis of an origami-inspired structure.

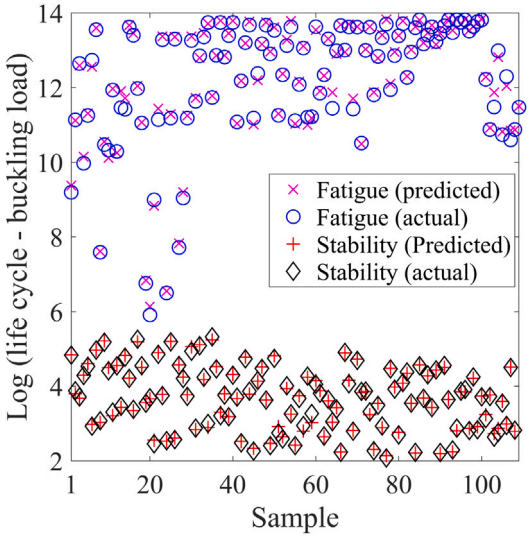

Fig. 4. Train vs. actual buckling loads and life cycle.

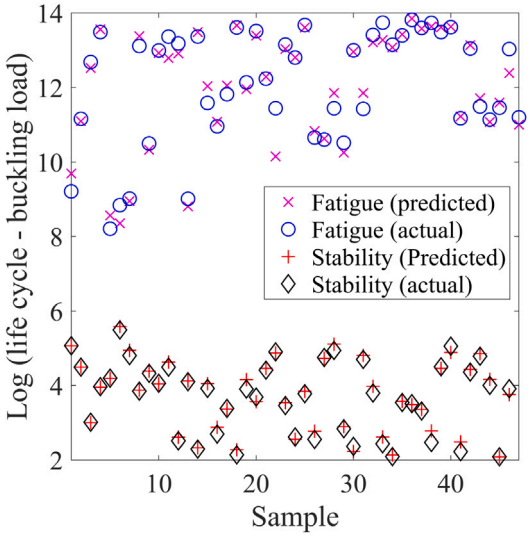

Fig. 5. Test vs. actual buckling loads and life cycle.

3. Results and discussions

This section comprises two sections. First, we discuss how the geometric parameters can improve or impair the stability of the inspired-origami structure. Next, we discuss the effect of these parameters on the fatigue and stability behavior of the structure simultaneously. We study the independent geometric parameters, including circumscribed circle's radius, total height, thickness, crease parameters (aspect and thickness ratios), length ratio, and story's height.

3.1. Stability analysis

This section outlines the effect of different geometric parameters on the buckling load of the inspired-origami structure using ANN results. Depending on how these geometric parameters are chosen, the stability of the structure may increase or be compromised, as shown in Figs. 6–16.

Figs. 6–7 depict the effect of b/a and R for different number of stories. In Fig. 6, the height of stories equals 50 mm for all cases. Other geometric parameters are considered as $\beta = 1$, $\alpha = 0.1$, $t = 2$, and R =

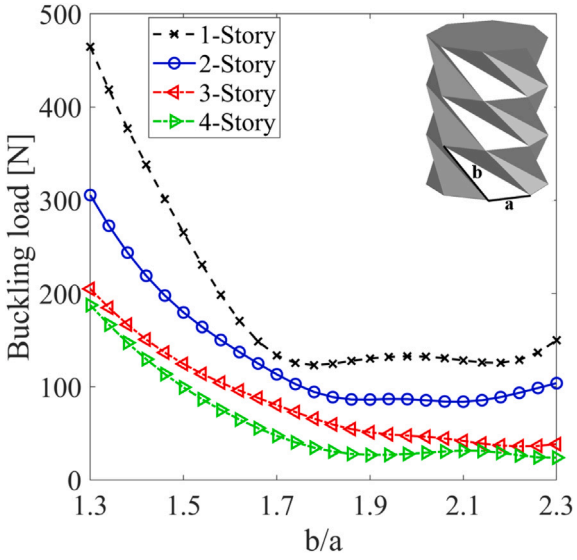

Fig. 6. Influence of b/a and number of stories on the stability.

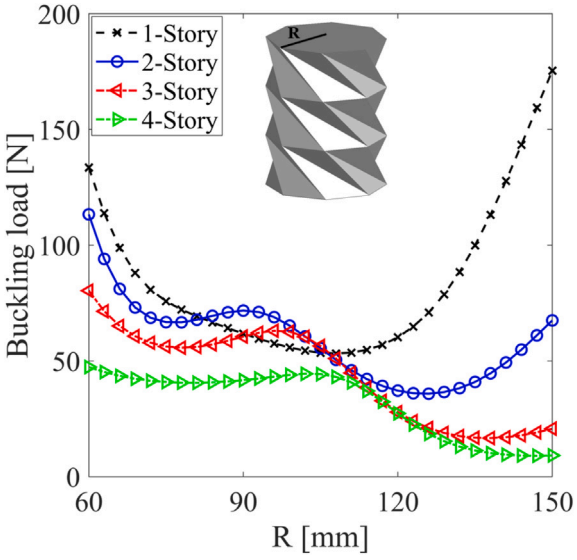

Fig. 7. Influence of R and number of stories on the stability.

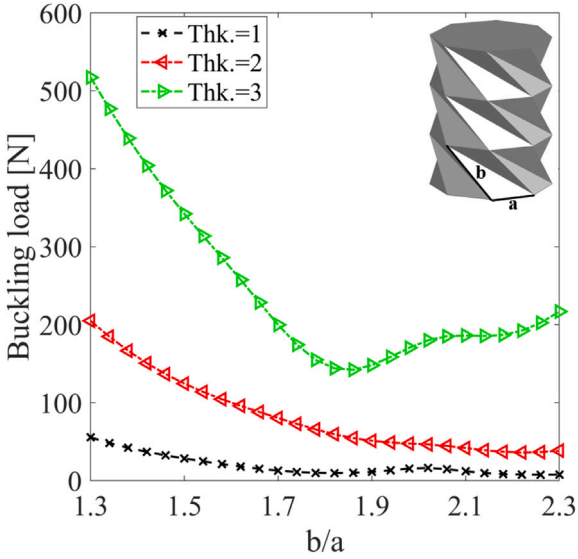

Fig. 8. Influence of b/a and $thk.$ on the stability of the structure.

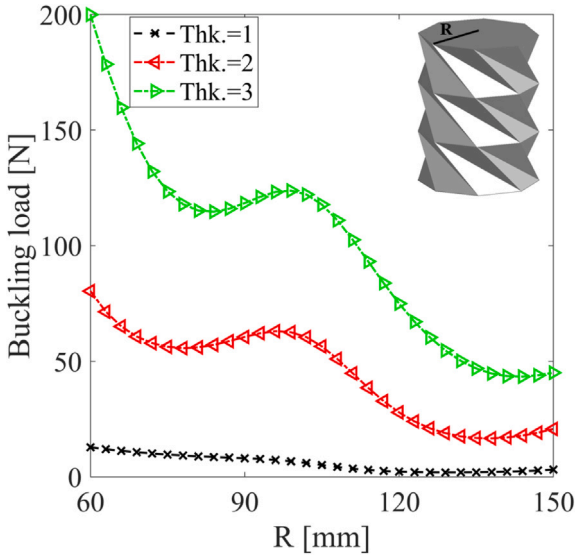

Fig. 9. Influence of R and $thk.$ on the stability of the structure.

60 mm. The results illustrate that the structural stability is improved by decreasing the value of b/a. The stability changes slightly when b/a is greater than 1.9. It is observed that the stability is decreased with the increase of stories. However, the difference between the buckling loads is slight when the structure consists of three and four stories.

Fig. 7 present origami structures with the geometric parameters of $\beta = 1$, $\alpha = 0.1$, thk. = 2 mm, and b/a = 1.7 . It is demonstrated that the structure is more stable when R is in the range of 60–120 mm. In this range, the buckling load is decreased by increasing R. When R is larger than 120 mm, the stability is improved slightly for the structure with two, three, and four stories. The stability improvement is significant for the one-story structure when R=120 or more.

Figs. 8–9 present the stability of the three-stories structure with different b/a and R, respectively. The structure is designed with considering $h = 50$ mm, $\beta = 1$, $\alpha = 0.1$, and thk. = 1, 2, and 3 mm. It can be found from these figures that the stability of the structure is enhanced with the increase of t. However, when b/a is changed in the range of 1.3 and 1.9 and thickness is 3 mm, the stability decreases significantly. The stability of the structure is somewhat constant for the b/a greater than 1.9 and thickness of 1 mm or 2 mm. It is shown in Fig. 9 that increasing the radius decreases the buckling load. The changes in the stability are slight for the structure with R of 125 mm or greater. As can be seen from both figures, with an increase in thickness, the difference between the buckling load increases substantially.

Fig. 10 displays the effect of b/a and R on the stability of the three-story structure designs. These designs include $\alpha = 0.1$, $\beta = 1$, $h = 50$ mm, and $t = 2$ mm. The stability is ameliorated with the decrease of b/a and R. The results show that this increase in stability is approximately uniform by varying these parameters. The stability is slightly improved around b/a of 1.9, but it decreases after this point. A similar pattern happens for the radius of 100 mm. The buckling load is increased significantly when b/a is changed from 1.7 to 1.3.

Figs. 11–12 present the influence of crease indexes and b/a on the buckling load of the proposed design. The structure comprises three stories with a radius of 60 mm and a story height of 50 mm. In Fig. 11 the thickness and β are 2 mm and 1, respectively. It is discovered that the stability of the structure is improved when α increases. This improvement is significant when b/a is 1.9 or more. It can be concluded

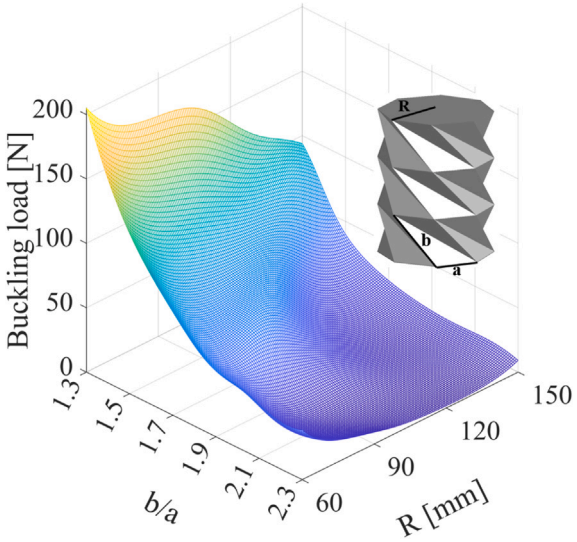

Fig. 10. Influence of R and b/a on the stability of the structure.

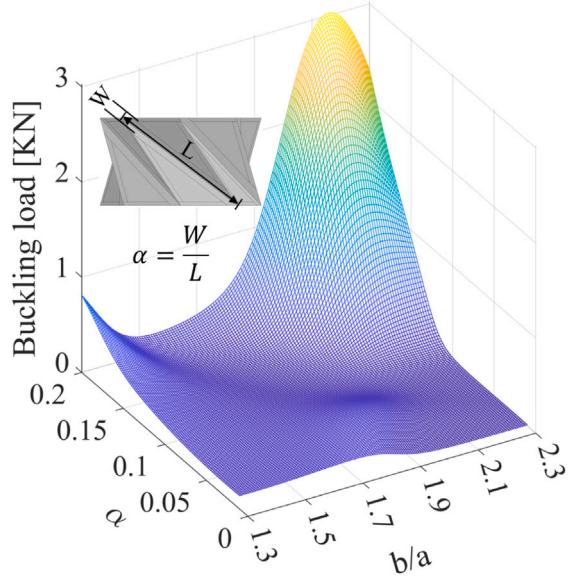

Fig. 11. Influence of α and b/a on the stability of the structure.

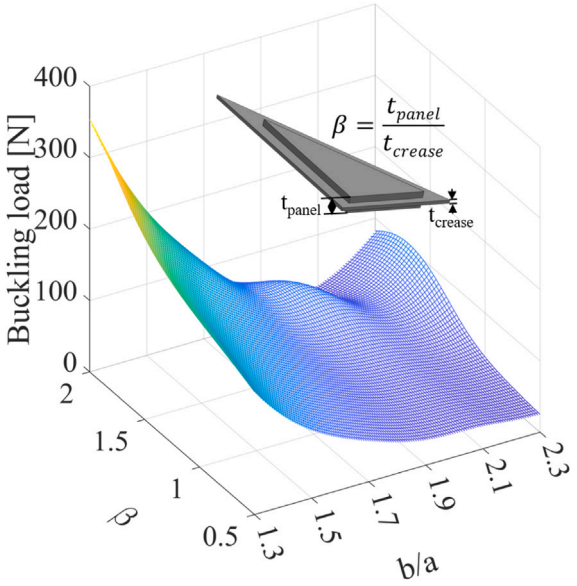

Fig. 12. Influence of β and b/a on the stability of the structure.

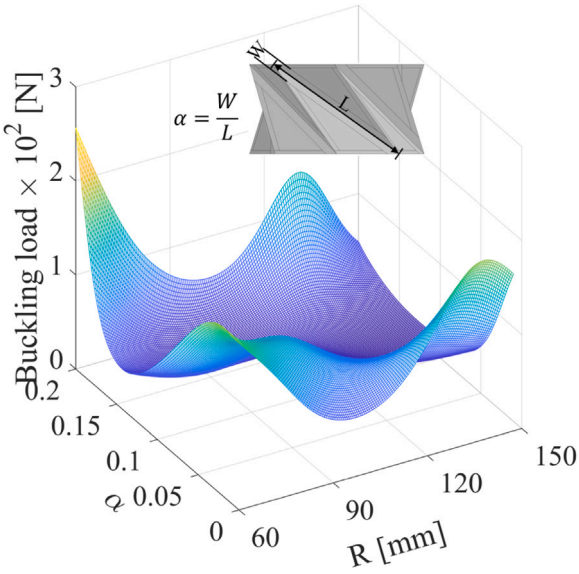

Fig. 13. Influence of α and R on the stability of the structure.

that increasing the width of flexible creases can increase the buckling load.

The α and thickness of creases are assumed to be 0.1 and 2 mm in Fig. 12. Increasing the thickness of the panel improves the stability for all length ratios (b/a). It means that the panels carry the majority of the stresses and the creases act like actuators. It proves that choosing a stiff material for panels and a flexible material for creases should be the best material selection in designing a Kresling origami-inspired structure.

Figs. 13–14 show the effect of creases indexes and the circumscribed circle's radius on the buckling load. This design includes three stories, and h and b/a are assumed to be 50 mm and 1.7. Based on these figures, $/alpha$ and $/beta$ affect the stability of the structure in accordance with R. When R is less than 90 mm, the stability of the structure is increased by increasing β. The buckling load is decreased with the increase of β for R greater than 90 mm. Fig. 13 indicates that first, the stability of the structure is lessened with the increase of α, then it is heightened when R is greater than 90 mm. When α is around 1.5, the buckling happens at the lowest applied force value for all cases. It is evident from the results that $/alpha$ and R should be considered simultaneously in determining the stability of the structure.

According to Figs. 15–16, the effect of H on the origami structure's stability is conditional on two other geometric parameters; b/a and R. This design has three stories with different heights, in which h varies from 17 mm to 70 mm. In this structure, t, α, and β are 2 mm, 0.1, and 1, respectively. It is demonstrated that the stability is improved with the decrease of b/a while H is 90 mm or more. When H is between 50 mm and 90 mm, the stability drops with the decrease of b/a from 1.9 to 1.7, then it is increased substantially. A similar trend happens when the total height is between 150 and 210 mm, and the length ratio is decreased from 1.7 to 1.5. The stability of the structure is enhanced extensively by decreasing R when H is greater than 150 mm. When the total height is between 50 mm and 90 mm, the increase of R enhances the stability of the structure.

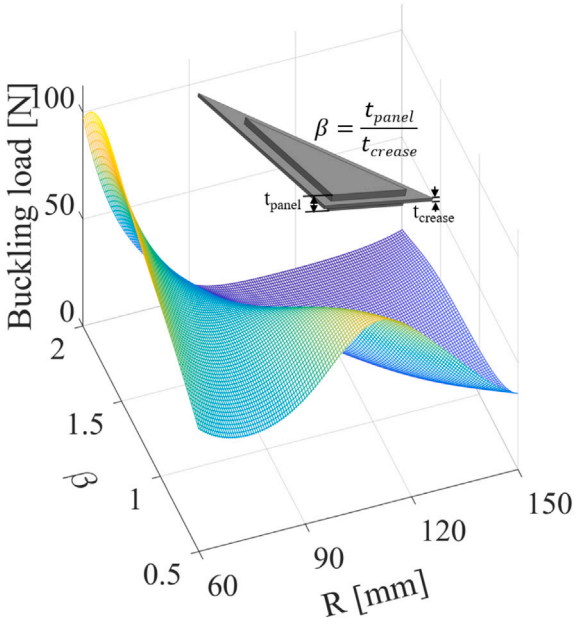

Fig. 14. Influence of β and R on the stability of the structure.

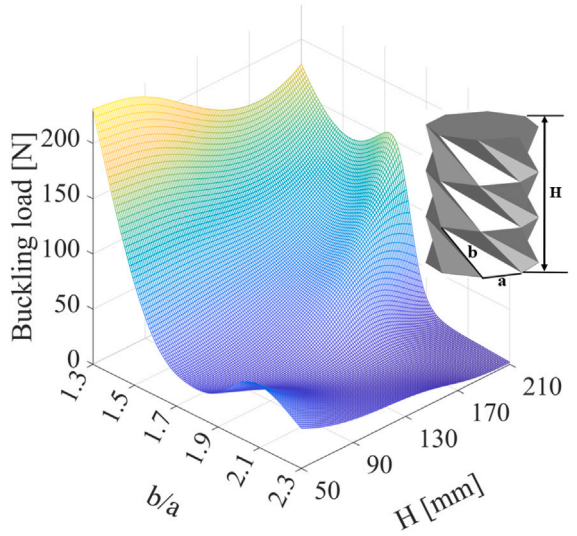

Fig. 15. Influence of H and b/a on the stability of the structure.

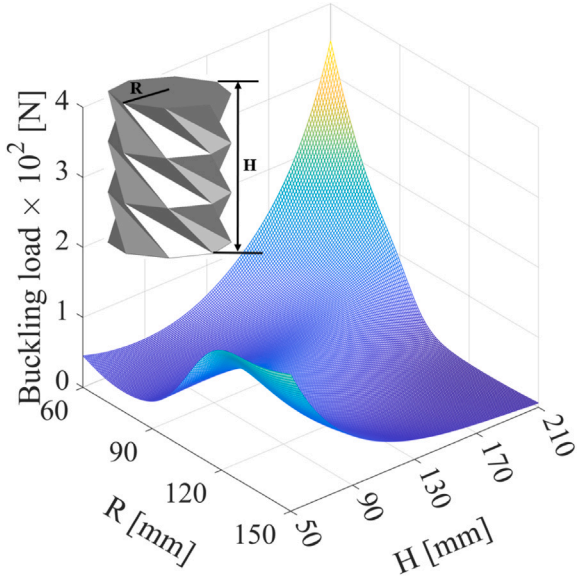

Fig. 16. Influence of H and R on the stability of the structure.

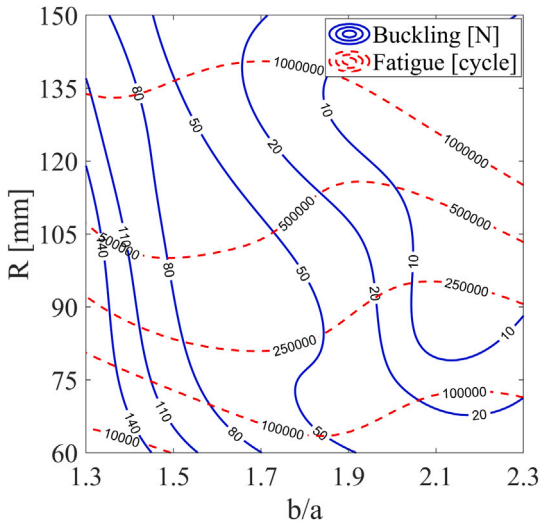

Fig. 17. Influence of R and b/a on the stability and fatigue failure of the structure.

3.2. Stability and fatigue prediction

This section explores how the designed structures' geometric parameters involve stability and fatigue failure. Therefore, providing the right range of these parameters is essential for improving the stability and fatigue life of the origami-inspired structure. Fatigue life and stability contours are plotted for b/a, R, H, α, and β in Figs. 17–19.

Fig. 17 presents how b/a and R change the stability and fatigue failure of the proposed design. It is illustrated that the life cycle and stability of the three-story structure are improved when b/a decreases and R increases simultaneously. It can be found that the structure has the optimum performance when b/a has a small value and R is large. The upper left of this figure is the optimum range of these two parameters. The stability of the structure is in jeopardy outside of this region. It is discovered that the influence of b/a on stability is more significant than the fatigue life. Although the fatigue life varies slightly with the change of b/a, its changes are significant with the variation of R.

Fig. 18 illustrates that when b/a and H are decreased, the stability and fatigue life of the structure are improved. In this figure, the structure contains three stories, and the total height varies from 50 mm to 210 mm. It is shown that when the length ratio is around 1.9, the changes in buckling load are slight. After this point, the stability of the structure is changed slightly with the increase of H, but the fatigue life is improved significantly. Although the stability is enhanced by decreasing the length ratio from 1.7 and increasing the total height, the fatigue failure happens at a lower cycle. The optimum values of these two parameters are determined in the figure's center region and right side.

It is explored from Fig. 19 that the optimum range of α and β is located in the upper right region of this figure. The structure's α and β vary between 0.01–0.2 and 0.5–2, respectively. The structure's life cycle is enhanced with the increase of α, and it reaches the maximum value when β is around 1 and 1.25. When α is greater than 0.15, the buckling load is increased significantly by increasing β. The difference between the buckling load is considerable with the increase of β, and α is less than 0.1. This figure shows two optimum stability regions, but

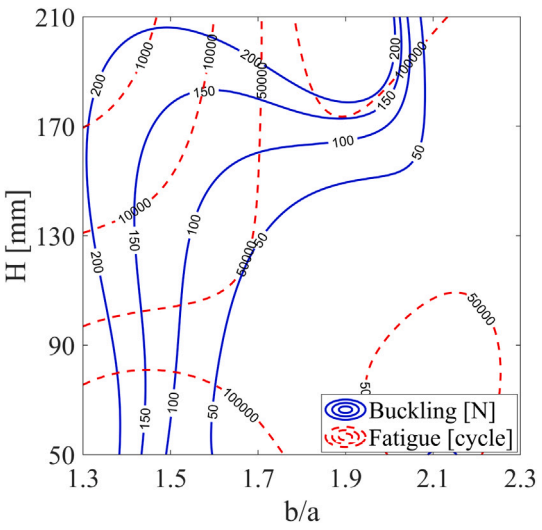

Fig. 18. Influence of H and b/a on the stability and fatigue failure of the structure.

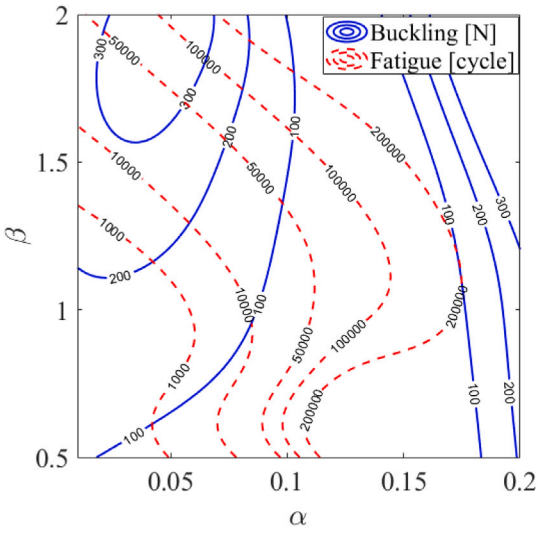

Fig. 19. Influence of β and α on the stability and fatigue failure of the structure.

the fatigue life is increased from the left to the right of the figure. It can be concluded that the ratio of width-to-length of creases plays a crucial influence on the mechanical behavior of the structure.

4. Conclusion

The fatigue failure and stability of a reconfigurable Kresling origami-inspired structure are investigated in this research. We utilize the mean stress with fully reversed loading to assess the structure's fatigue failure. The nonlinear-based eigenvalue approach is used to evaluate the stability of the structure. Our study explores the mechanical properties of an origami-inspired structure using flexible crease sections and stiff panels.

In terms of computational efficiency, using FEA to investigate how geometric parameters influence the mechanical properties of an origami structure is expensive. This led us to develop an ANN model that could estimate a broader range of parameters for the stability and life cycle of the structure. The ANN was trained using a set of seven parameters: circumscribed circle's ratio of polygonal, total height, thickness, crease parameters (aspect and thickness ratios), length ratio, and story's height. Using random sampling, we divided the FEM dataset into training (70% of the data) and test sets (30% of the data).

It is indicated that these parameters have a significant impact on the mechanical properties of origami designs. We can conclude that the structure is more stable when b/a and R are reduced. Whenever the number of stories increases, there is a corresponding decrease in the stability. Despite the fact that buckling load increases as the height is decreased, its effect is dependent on the circumscribed circle's radius and the length ratio.

Panels constructed of stiff materials and creases constructed of flexible materials can enhance the folding performance of the structure. This study demonstrates that the effect of crease indexes on the mechanical properties of a structure depends on the value of R, while an increase in the value of $alpha$ results in a delay in buckling. In addition, it is found that panels bear the greatest load on the origami-inspired structure, resulting in a considerable effect on its stability.

Furthermore, we observe the effects of these parameters on the structure's stability and life cycle at the same time. It is found that structures with a large b/a and a small R have the best performance among different cases. The life cycle and stability can be enhanced by reducing the length ratio as well as the height. It is discovered that the structure's performance is improved by increasing the aspect ratio and keeping the thickness ratio between 1 and 1.25. In addition, to improve the structure's stability and life cycle, the creases can be made wider so that they can change their state with less effort.

CRediT authorship contribution statement

Mojtaba Moshtaghzadeh: Conducted simulations and processed the data, Generated the figures, Wrote the text in multiple iterations, Developed the idea, Supervision. **Ali Bakhtiari:** Conducted simulations and processed the data, Wrote the text in multiple iterations. **Pezhman Mardanpour:** Wrote the text in multiple iterations, Developed the idea, Supervision.

Declaration of competing interest

The authors declare that they have no known competing financial interests or personal relationships that could have appeared to influence the work reported in this paper.

Data availability

No data was used for the research described in the article.

Acknowledgments

The Air Force Office of Scientific Research (AFOSR) and the U.S. National Science Foundation (NSF) support Professor Mardanpour's research under grants FA9550-18-1-0191 and 1934749. We would like to express our special appreciation and thanks to professor Stavros V. Georgakopoulos for his support and help about the origami antenna structure.

References

[1] Puig L, Barton A, Rando N. A review on large deployable structures for astrophysics missions. Acta Astronaut 2010;67(1–2):12–26.
[2] Sareh P, Chermprayong P, Emmanuelli M, Nadeem H, Kovac M. Rotorigami: A rotary origami protective system for robotic rotorcraft. Science Robotics 2018;3(22).
[3] Bobbert F, Janbaz S, van Manen T, Li Y, Zadpoor A. Russian doll deployable meta-implants: Fusion of kirigami, origami, and multi-stability. Mater Des 2020;191:108624.
[4] Li S, Fang H, Sadeghi S, Bhovad P, Wang K-W. Architected origami materials: how folding creates sophisticated mechanical properties. Adv Mater 2019;31(5):1805282.

[5] Zekios CL, Liu X, Moshtaghzadeh M, Izadpanahi E, Radnezhad HR, Mardanpour P, Georgakopoulos SV. Electromagnetic and mechanical analysis of an origami helical antenna encapsulated by fabric. In: ASME 2019 international design engineering technical conferences and computers and information in engineering conference. American Society of Mechanical Engineers Digital Collection; 2019.

[6] Thrall A, Quaglia C. Accordion shelters: A historical review of origami-like deployable shelters developed by the US military. Eng Struct 2014;59:686–92.

[7] Lebée A. From folds to structures, a review. Int J Space Struct 2015;30(2):55–74.

[8] Meloni M, Cai J, Zhang Q, Sang-Hoon Lee D, Li M, Ma R, Parashkevov TE, Feng J. Engineering Origami: A comprehensive review of recent applications, design methods, and tools. Adv Sci 2021;2000636.

[9] Pesenti M, Masera G, Fiorito F. Exploration of adaptive origami shading concepts through integrated dynamic simulations. J Archit Eng 2018;24(4):04018022.

[10] Lee J-Y, Kang BB, Lee D-Y, Baek S-M, Kim W-B, Choi W-Y, Song J-R, Joo H-J, Park D, Cho K-J. Development of a multi-functional soft robot (SNUMAX) and performance in RoboSoft Grand Challenge. Front Robot AI 2016;3:63.

[11] Zirbel SA, Trease BP, Thomson MW, Lang RJ, Magleby SP, Howell LH. Hanaflex: a large solar array for space applications. In: Micro-and nanotechnology sensors, systems, and applications vii, vol. 9467. International Society for Optics and Photonics; 2015, p. 94671C.

[12] Yuan L, Shi H, Ma J, You Z. Quasi-static impact of origami crash boxes with various profiles. Thin-Walled Struct 2019;141:435–46.

[13] Wu J, Long Y, Zhou Y, Yu Y, Liu J, et al. Experimental study on the deformation and damage of cylindrical shell-water-cylindrical shell structures subjected to underwater explosion. Thin-Walled Struct 2018;127:654–65.

[14] Filipov ET, Tachi T, Paulino GH. Origami tubes assembled into stiff, yet reconfigurable structures and metamaterials. Proc Natl Acad Sci 2015;112(40):12321–6.

[15] Yang K, Xu S, Shen J, Zhou S, Xie YM. Energy absorption of thin-walled tubes with pre-folded origami patterns: Numerical simulation and experimental verification. Thin-Walled Struct 2016;103:33–44.

[16] Yoshimura Y. On the mechanism of buckling of a circular cylindrical shell under axial compression. NACA Tech Memo 1955;1390.

[17] Lord GJ, Champneys AR, Hunt GW. Computation of homoclinic orbits in partial differential equations: an application to cylindrical shell buckling. SIAM J Sci Comput 1999;21(2):591–619.

[18] Guest SD, Pellegrino S. The folding of triangulated cylinders, Part I: Geometric considerations. J Appl Mech 1994;61(4):773–7.

[19] Jianguo C, Xiaowei D, Ya Z, Jian F, Yongming T. Bistable behavior of the cylindrical origami structure with Kresling pattern. J Mech Des 2015;137(6):061406.

[20] Kresling B. Folded tubes as compared to kikko (" tortoise-shell55) bamboo. Origami 2002;3:197.

[21] Kresling B, Abel JF. Natural twist buckling in shells: from the hawkmoth's bellows to the deployable Kresling-pattern and cylindrical Miura-ori, in: Proceedings of the 6th international conference on computation of shell and spatial structures, John F. Abel and J. Robert Cooke, Eds., Ithaca, vol. 11, 2008, pp. 12–32.

[22] Jianguo C, Xiaowei D, Yuting Z, Jian F, Ya Z. Folding behavior of a foldable prismatic mast with Kresling origami pattern. J Mech Robot 2016;8(3):031004.

[23] Li J, Chen Y, Feng X, Feng J, Sareh P. Computational modeling and energy absorption behavior of thin-walled tubes with the Kresling origami pattern. J Int Assoc Shell Spat Struct 2021;62(2):71–81.

[24] Masana R, Daqaq MF. Equilibria and bifurcations of a foldable paper-based spring inspired by Kresling-pattern origami. Phys Rev E 2019;100(6):063001.

[25] Phocas MC, Christoforou EG, Dimitriou P. Kinematics and control approach for deployable and reconfigurable rigid bar linkage structures. Eng Struct 2020;208:110310.

[26] Kaveh A, Bakhshpoori T. Metaheuristics: outlines, MATLAB codes and examples. 2019.

[27] Salehzadeh R, Nejad FB, Shamshirsaz M. Vibration control of a rotating cantilever beam using piezoelectric actuator and feedback linearization method. 2020, arXiv preprint arXiv:2004.11703.

[28] Chen Y, Sareh P, Yan J, Fallah AS, Feng J. An integrated geometric-graph-theoretic approach to representing origami structures and their corresponding truss frameworks. J Mech Des 2019;141(9).

[29] Tachi T. Simulation of rigid origami. Origami 2009;4(08):175–87.

[30] Filipov E, Liu K, Tachi T, Schenk M, Paulino GH. Bar and hinge models for scalable analysis of origami. Int J Solids Struct 2017;124:26–45.

[31] Gillman A, Fuchi K, Buskohl P. Truss-based nonlinear mechanical analysis for origami structures exhibiting bifurcation and limit point instabilities. Int J Solids Struct 2018;147:80–93.

[32] Zhu Y, Filipov ET. A bar and hinge model for simulating bistability in origami structures with compliant creases. J Mech Robot 2020;12(2).

[33] Chen Y, Feng J. Folding of a type of deployable origami structures. Int J Struct Stab Dyn 2012;12(06):1250054.

[34] Hernandez EAP, Hartl DJ, Akleman E, Lagoudas DC. Modeling and analysis of origami structures with smooth folds. Comput Aided Des 2016;78:93–106.

[35] Chen Y, Fan L, Bai Y, Feng J, Sareh P. Assigning mountain-valley fold lines of flat-foldable origami patterns based on graph theory and mixed-integer linear programming. Comput Struct 2020;239:106328.

[36] Qiu C, Zhang K, Dai JS. Repelling-screw based force analysis of origami mechanisms. J Mech Robot 2016;8(3):031001.

[37] Moshtaghzadeh M, Izadpanahi E, Mardanpour P. Stability analysis of an origami helical antenna using geometrically exact fully intrinsic nonlinear composite beam theory. Eng Struct 2021;234:111894.

[38] Hodges DH. Geometrically exact, intrinsic theory for dynamics of curved and twisted anisotropic beams. AIAA J 2003;41(6):1131–7. http://dx.doi.org/10.2514/2.2054.

[39] Moshtaghzadeh M, Bakhtiari A, Izadpanahi E, Mardanpour P. Artificial Neural Network for the prediction of fatigue life of a flexible foldable origami antenna with Kresling pattern. Thin-Walled Struct 2022;174:109160. http://dx.doi.org/10.1016/j.tws.2022.109160.

[40] Moshtaghzadeh M, Izadpanahi E, Mardanpour P. Prediction of fatigue life of a flexible foldable origami antenna with Kresling pattern. Eng Struct 2022;251:113399.

[41] Moshtaghzadeh M, Bakhtiari A, Izadpanahi E, Mardanpour P. Stability and fatigue analysis of an adaptive origami antenna structure with Kresling pattern. In: AIAA SCITECH 2022 forum. 2022, p. 0921.

[42] Fan W, Chen Y, Li J, Sun Y, Feng J, Hassanin H, Sareh P. Machine learning applied to the design and inspection of reinforced concrete bridges: Resilient methods and emerging applications. In: Structures, vol. 33. Elsevier; 2021, p. 3954–63.

[43] Chen RJ, Lu MY, Chen TY, Williamson DF, Mahmood F. Synthetic data in machine learning for medicine and healthcare. Nat Biomed Eng 2021;5(6):493–7.

[44] Rezamand M, Kordestani M, Carriveau R, Ting DS, Orchard ME, Saif M. Critical wind turbine components prognostics: A comprehensive review. IEEE Trans Instrum Meas 2020.

[45] Brunton SL, Kutz JN. Data-driven science and engineering: Machine learning, dynamical systems, and control. Cambridge University Press; 2022.

[46] Gopal M. Applied machine learning. McGraw-Hill Education; 2019.

[47] Liu T, Wang Z, Zeng J, Wang J. Machine-learning-based models to predict shear transfer strength of concrete joints. Eng Struct 2021;249:113253.

[48] Zhang P, Fan W, Chen Y, Feng J, Sareh P. Structural symmetry recognition in planar structures using Convolutional Neural Networks. Eng Struct 2022;260:114227.

[49] Liu Z, Fang H, Xu J. Identification of piecewise linear dynamical systems using physically-interpretable neural-fuzzy networks: Methods and applications to origami structures. Neural Netw 2019;116:74–87.

[50] Yasuda H, Yamaguchi K, Miyazawa Y, Wiebe R, Raney JR, Yang J. Data-driven prediction and analysis of chaotic origami dynamics. Commun Phys 2020;3(1):1–8.

[51] Bhovad P, Li S. Physical reservoir computing with origami and its application to robotic crawling. Sci Rep 2021;11(1):1–18.

[52] Ansys® academic research mechanical, theory reference. ANSYS, Inc.; 2021.

[53] Bhashyam GR. ANSYS mechanical—a powerful nonlinear simulation tool, vol. 1. (1):Ansys, Inc; 2002, p. 39.

[54] Wang B, Lu H, Kim G-h. A damage model for the fatigue life of elastomeric materials. Mech Mater 2002;34(8):475–83.

[55] Amjadi M, Fatemi A. Creep and fatigue behaviors of High-Density Polyethylene (HDPE): Effects of temperature, mean stress, frequency, and processing technique. Int J Fatigue 2020;141:105871.

[56] He W, Williard N, Chen C, Pecht M. State of charge estimation for Li-ion batteries using neural network modeling and unscented Kalman filter-based error cancellation. Int J Electr Power Energy Syst 2014;62:783–91.

[57] Ashtiani F, Geers AJ, Aflatouni F. Single-chip photonic deep neural network for instantaneous image classification. 2021, arXiv preprint arXiv:2106.11747.